

Review

The MRI-Model in Sputter Depth Profiling: Capabilities, Limitations and Recent Progress

Siegfried Hofmann* and Jiang Yong Wang

Max-Planck-Institute for Metals Research Heisenbergstr.3 70569 Stuttgart, Germany

*s.hofmann@mf.mpg.de

(Received: February 5, 2006 ; Accepted: May 31, 2006)

After an outline of the basic structure of the MRI model for quantification of sputter depth profiles and the working scheme for profile reconstruction, a few examples show its application potential and the usefulness of some extensions. The shape of a GDOES depth profile can be well represented, showing sub-monolayer depth resolution. An extension for a tilted sample in front of a cylindrical mirror analyzer is reevaluated showing a small but measurable effect. Inclusion of preferential sputtering of one component is demonstrated for depth profiling of a Ni/Cr multilayer with nitrogen ions, and finally the result of a modification by elastic electron backscattering in AES depth profiling is shown for a C/Ta bilayer.

1. Introduction

Quantitative surface analysis in case of sputter depth profiling has to be extended to the case of sputtering induced changes of surface morphology and surface composition.

From the very beginning of surface analysis at the end of the sixties of last century, quantification of surface analysis was a steady issue and is only nowadays approaching its experimentally determined limit in the low percentage range. Kazuhiro Yoshihara was one of the first among the researchers in the field that were pushing forward national and international cooperation necessary to establish firm data bases for further improvement, and he created the common data processing system for surface analysis [1]. Because of the general presence of native oxide layers and of the influence of any surface cleaning methods on surface composition, for example sputter cleaning and/or heating, establishment of a well defined surface composition is not an easy task. Mechanical cleavage or scratching often is the best way to achieve that. Nevertheless, in principle quantitative surface analysis can be performed without changing the surface composition. In contrast, quantification of sputter depth profiles means quantification by taking into account a steadily changing surface composition and morphology, induced by the action of energetic ion bombardment. Therefore, quantitative depth profiling has to be based on some kind of model description of the sputtering induced change in surface composition and morphology to be able to reconstruct the original depth distribution from the measured profile. One of the first attempts to do so was the so-called

sequential layer sputtering (SLS) model, originally introduced by Benninghoven (1971) [2] and later adapted by Hofmann (1976) [3] to describe the development of profile broadening with sputtered depth. It became soon clear that some modifications were necessary [4] to make it universally applicable. Although it still has some merits in describing profile development in the first few monolayers as well as the sputtering induced roughness in case of polycrystalline samples, its basic flaw is that it only takes into account surface roughening and information depth but omits atomic mixing. Finally, by putting together the combined action of atomic mixing, roughness and information depth into one model, the first steps of the mixing-roughness-information depth (MRI) model were created [5,6,7]. A detailed description together with a thorough experimental test was published in 1993 [8], reporting sputter depth profiles of an Al/As multilayer with 10 nm single layer thickness, a pre-runner of the nowadays ISO standard sample with 20 nm layer thickness [9]. The model was refined later, in particular while one of the authors (S. H.) was at the National Research Institute for Metals (NRIM, now NIMS) in Tsukuba, Japan [10] and implemented in the COMPRO software of the Surface Analysis Society of Japan [11]. Further extensions and modifications followed and are still going on [12, 13,] and after his return to Stuttgart. In the following, capabilities and limitations of the MRI model are outlined and briefly discussed.

2. Outline and Modifications of the MRI Model

2.1 Basic structure

Provided that the basic conversions of intensity (I) to

concentrations (X) and of sputtering time to sputtered depth (z) have already been done [6], a simple mathematical description of the action of sputter depth profiling on the original in depth distribution of composition, is possible by the so-called convolution integral [10]:

$$I(z)/I(0) = \int_{-\infty}^{+\infty} X(z') \cdot g(z-z') dz' \quad (1)$$

that gives the measured and normalized intensity at the sputtered depth z, I(z)/I(0), as a function of the original in depth distribution of composition, X(z') by action of the depth resolution function(DRF), g(z-z'). Deconvolution means solving eqn (1) for X(z') which is possible e.g. by inverse Fourier transformation schemes if g(z-z') and I(z)/I(0) are known. Because of practical problems with that approach [14] it is customary to solve the problem by "forward calculation" of the convolution eqn. (1), i.e. assuming a suitable X(z') and comparing the calculated profile with the measured profile I(z)/I(0). By changing the input X(z') until an optimum fit is obtained, the "original" in-depth distribution of composition is finally reconstructed [10]. The DRF contains the physical parameters determining the "response" of the system under study in terms of the measured profile.

The MRI- model provides a mathematical description of the DRF g(z-z') that is composed of three partial DRF's based on the three fundamental contributions atomic mixing (g_w), surface roughness (g_σ), and information depth (g_λ). These contributions are given by physically well defined parameters and their dependencies with depth [15-18]: Atomic mixing is described by an exponential function with a characteristic mixing zone length, w,

$$g_w = \frac{1}{w} \exp[-z(z-z'+w)/w] \quad (2)$$

the information depth by another exponential function with a characteristic length λ,

$$g_\lambda = \frac{1}{\lambda} \exp[-z(z-z')/\lambda] \quad (3)$$

and the roughness by a Gaussian term with standard deviation σ (corresponding to rms roughness on a surface),

$$g_\sigma = \frac{1}{\sqrt{2\pi}\sigma} \exp\left[-\frac{(z-z')^2}{2\sigma^2}\right] \quad (4)$$

These functions constitute the total depth resolution function g(z-z') in eq. (1). They are sequentially employed to the (assumed) depth distribution of an element, given by thin layers each with (different) concentrations. For example, each monoatomic layer at a location z₀ gives a normalized contribution at a sputtered depth z of the shape of the depth resolution function.

Based on these three physical parameters, the MRI model

allows a mathematical extraction of the DRF that can in turn be applied to fit a measured profile by solving equ. (1), i.e. first assuming and then changing the original in-depth distribution, X(z'), until an optimum fit is obtained. Fig. 1 shows schematically the described procedure. The establishment of the DRF is possible by theoretical prediction (for w and λ, at least within a certain error margin) and/or experimentally by profiling of well known reference samples of not too different composition as compared to the unknown sample.

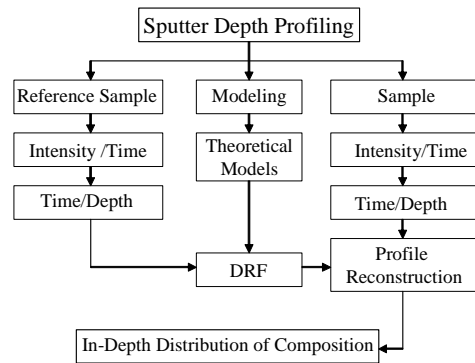


Fig. 1 Working scheme of quantification of sputter depth profiles with depth resolution function (DRF) according to the MRI model. For details see text.

Note that in contrast to other "empirical" DRFs particularly used in SIMS, the MRI parameters have a well defined physical meaning, and therefore they can be theoretically predicted and/or experimentally measured by independent methods. For example, the information depth parameter λ is represented here by the attenuation length of the respective Auger- or photo electrons in AES and XPS (note that usually, the information depth is defined by 3λ or 5λ). In SIMS, the information depth corresponds to the secondary ion escape depth (about 1-2 ML). The mixing length is at least approximately predicted by the TRIM (or SRIM) codes (ion ranges or better mean range of total recoil displacements) and can be independently measured by angle resolved AES or XPS, as shown for ARAES in ref.[15]. Roughness is hard to predict, but surface roughness after profiling can be measured by AFM, and original interface roughness by grazing incidence X-ray reflectometry (GIXR) [16]. However, "straggling" of the mixing length causes an additional roughness term that is difficult to estimate, but should be less than the mixing length. Note that the linear description pointed out above is a first order approximation. In principle, the effect of the parameters w and λ on the intensity are not independent and have to be taken into account by a suitable "Ansatz", as pointed out in ref. [17].

The MRI model has proved its usefulness in depth profiling using AES, XPS and SIMS [18]. For example, a comparative study of the profile quantification of an AlAs double

layer structure with both techniques proved its applicability with the same atomic mixing parameter according to the same ion species (Ar^+), and similar incidence [19]. The favorable employment of “backside sputtering” in SIMS takes advantage of the asymmetric DRF, meaning that the front of a profile is better resolved than the backside. This leads to better depth resolution even at higher w values when profiling from both sides as demonstrated by Yeo et al. [20, 21]. How to extract roughness and mixing parameters as a function of ion energy in SIMS results using the MRI model has been shown by Takano et al. [22].

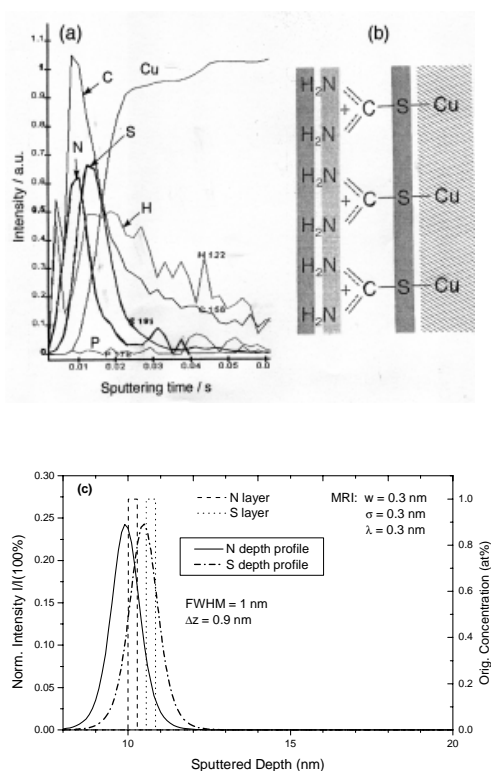


Fig. 2 (a) GDOES depth profile of a thiourea monolayer on Cu. (from ref. 23, courtesy of K. Shimizu). (b) Structure of the surface layer. (c) MRI fit of the N and S peaks in the GDOES depth profile of (a).

An example of fitting GDOES (Glow Discharge Optical Emission Spectroscopy) depth profiles with the MRI model is shown in Fig. 2a,b,c. Fig. 2a shows the GDOES depth profile of a monolayer of Thiourea (structure shown in 2b) on a smooth copper surface published by K. Shimizu et al. [23]. It is interesting to note that the depth resolution is high enough to separate the N and S peaks that are only separated by carbon, i.e. about 2 monolayers apart, as seen in the diagram of the structure. Because of the very low ion energy in GDOES (about 50 eV), the mixing parameter is expected to be of the order of the theoretical limit, i.e. 0.3 nm [24]. The information depth parameter, as in SIMS, should be again

about one monolayer (ca. 0.3 nm). Since the sputtering induced roughness should be zero at sputtering time zero, we assume conservatively again about 0.3 nm for the 3rd and 5th monolayer. The result is shown in Fig. 2c that gives a reasonable image of the normalized N and S peak shapes observed, with an estimated sputtering rate of about 1 nm/ms. The resulting depth resolution is about 0.9 nm.

The basic capability of the MRI model is the quantification of sputter depth profiles by profile reconstruction. In favorable cases, the precision is better than 0.2 ML [13]. Furthermore, the MRI parameters can be evaluated by fitting the results to measured profiles of well-defined reference samples. By separation of their influences on depth resolution, clear guidelines of the influences on depth resolution can be established.

The basic limitations of the MRI model lie, of course, in its simplicity. In its original form, it does not take into account preferential sputtering and other nonlinearities, for example in the intensity/concentration relation. Therefore several modifications were introduced to consider quantitatively some of these phenomena.

2.2 Extensions and Modifications

AES depth profiles are frequently performed using a CMA (Cylindrical Mirror Analyzer) [8, 25]. Only for the case of the CMA axis being normal to the sample surface, there is a unique escape depth (λ) value for all the electrons getting into the analyzer around the azimuthal circumference of the acceptance cone with the angle $\phi_A = 42.3^\circ$. Therefore, the electron escape depth is $\lambda = \lambda_0 \cdot \cos \phi_A = 0.74 \cdot \lambda_0$, with λ_0 the attenuation length (e.g. from NIST tables, [ref]). However, when the sample is tilted in front of the analyzer, an average $\cos \phi_{av}$ can be calculated as a function of the tilt angle, α , [see Fig. 4.2 in ref. 26] This relation applies for the respective average escape depth that is used in MRI profile calculations [8]. As pointed out by Bungo et al. [25], this procedure does not take into account the response of the MRI model to different escape depths around the azimuth angle of the analyzer, and averaging has to be performed after each MRI calculation for different angles. Following the extension given by Bungo et al., a typical sputter depth profile of a layer of 20 nm thickness was calculated, with dominating λ influence, and the result was compared with the original model calculated with the average of $\lambda_{av} = \lambda_0 \cdot \cos \phi_{av}$ [26].

An example is shown in Fig. 3a for the “critical” angle $\alpha_c = 47.7^\circ$, with λ_0 assumed to be 5 nm, a rather high value. Even for this condition and with w and σ almost negligible, the deviation of the simple and the extended model is relatively small. As seen in Fig. 3b [27] the deviation near the intensity maximum is 3.5% for the worst case at the critical angle (that is when the analyzer uptake cone touches the surface plane, and shadowing of the lower part of the CMA starts for higher tilt angles). For lower tilt angles, it is rapidly decreasing to

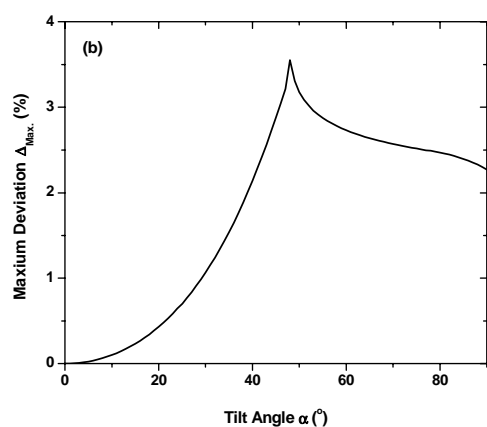
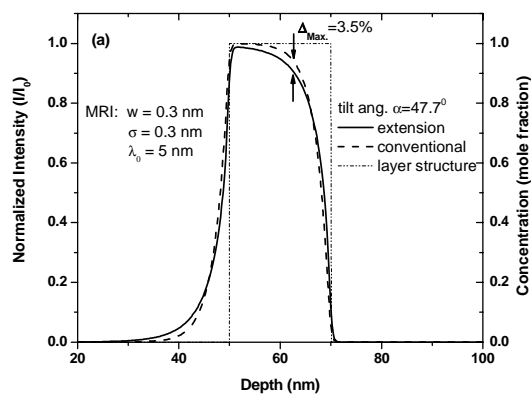


Fig. 3 (a) AES depth profile with a CMA instrument: Comparison of the result of an MRI extension with respect to different electron escape depth with the same result when using an average value for the escape depth shown in ref. 26. Layer thickness 20 nm, MRI parameter in the inset, tilt angle α between analyzer axis and normal to the sample surface is the critical angle, 47.7° . (b) Dependence of the maximum deviation (in % of the normalized intensity) on the tilt angle α .

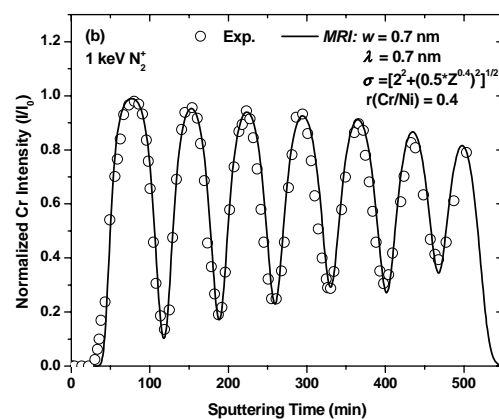
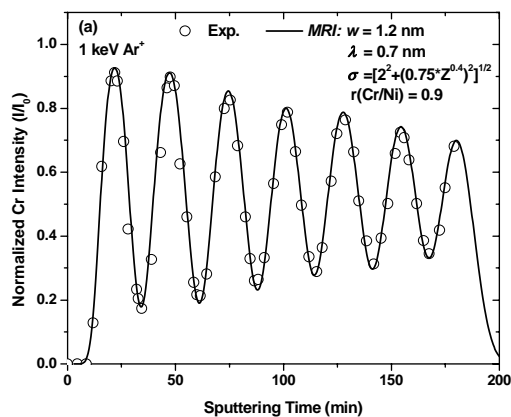


Fig. 4 Depth profiles of Cr for a Ni/Cr multilayer sample with about 11.5 nm single layer. Depth, (a) for sputtering with 1 keV Ar^+ ions, (b) with 1 keV N_2^+ ions. MRI Calculations include a depth dependent σ value and the sputtering rate ratio of Cr to Ni, $r(\text{Cr}/\text{Ni})$.

zero and less than 1 % at 30° . For higher angles, e.g. $>60^\circ$, it is about 2.5 %. In view of the accuracy of the attenuation length and of the usual error margin in AES depth profiling it seems that this deviation should not be overestimated, but it will certainly be necessary for high precision measurements. Of course, with the simple approach one cannot simply take the NIST table value of the attenuation length, λ_0 , as used for comparison in ref. [25], but $\lambda_0 \cdot \cos \phi_{av}$.

During the past years, the MRI model has been extended by several modifications. The first one is rather straight forward and concerns introduction of the often found depth dependence of the roughness parameter, σ [28], as seen in Fig. 4.

The specific dependencies of the MRI parameters on the

instantaneous composition play a major role in understanding depth profiling results. These dependencies can explain profile shape changes that are caused by nonlinear behavior with concentration [19], by matrix dependent changes of the mixing parameter [12] and of the information depth at interfaces [13]. The latter was experimentally shown by Prieto et al [29]. While the influence of the variations of these parameters appears to be small, nonlinearities in the sputtering time/sputtered depth relation are most important, as encountered when there is preferential sputtering of a component [30]. Assuming a linear dependence of the sputtering rate on surface composition, this relation can easily be introduced in the MRI model. In this way, the shape of a Ta/Si multilayer profile was correctly predicted

when a sputtering rate ratio of pure Si to pure Ta of 3.5 was assumed [30]. An example of the Cr profile calculation in the case of a Ni/Cr multilayer structure sputtered with 1keV Ar⁺ and with 1 keV N₂⁺ ions [31] is shown in Fig. 4. While for Ar⁺ sputtering the sputtering rate difference is almost negligible ($r(\text{Cr}/\text{Ni}) = 0.9$, Fig. 4a), for N₂⁺ sputtering, the sputtering rate of Cr is more than a factor of 2 lower than that of Ni ($r(\text{Cr}/\text{Ni}) = 0.4$), leading to the typical “deformed” shape of the intensity/sputtering time profile shown in Fig 4b.

3. New Developments

In order to enlarge the capabilities of the MRI model, a few modifications of the MRI model have already been introduced. Further progress is expected by introducing a changing mixing parameter to be able to better describe the transient zone in a profile at the beginning [27]. Recently, the effect of elastic electron backscattering on the shape of the depth profile of a Carbon layer on Tantalum was successfully treated with the MRI model by application to the apparently altered profile [32]. Using a simple exponential relation for the intensity with respect to the distance to the interface given in ref. [33], it was possible to model several depth profiles where the backscattering effect was of strong influence [27]. An example is shown in Fig. 5, where the profile of C at a C/Ta bilayer shown in Fig. 2a of ref. [32] is depicted together with the MRI result of the calculated profile. For the 3 keV primary electrons, the characteristic backscattering length was found to be $l_B = 27$ nm. The MRI parameters are shown in the inset of Fig. 5.

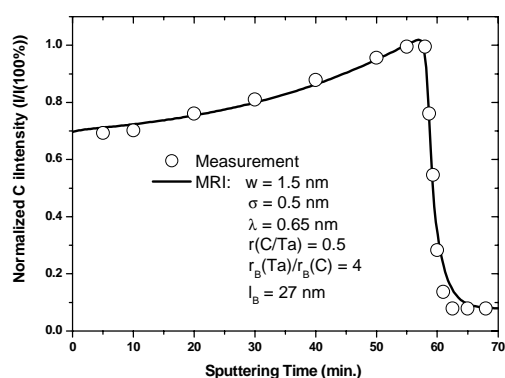


Fig. 5 C profile of a C/Ta bilayer, showing the effect of electron backscattering by Ta in the experimental data and their fit with the MRI model. The ratio of backscattering of Ta and C is $r_B(\text{Ta})/r_B(\text{C})=4$.

4. Summary and Outlook

The MRI model, based on the three physical parameters atomic mixing, roughness and information depth, has been developed as a versatile tool for profile reconstruction ap-

plicable to all sputtering depth profiles, e.g. obtained by AES, XPS, SIMS, GDOES etc. with a typical accuracy in the submonolayer regime and a precision only limited by the signal to noise ratio of the measurements. The MRI model provides quantitative information even in the case of non-linear dependencies between concentration and signal intensity and between sputtered depth and sputtering time, as for the occurrence of preferential sputtering of one component. Basic limitations of the model are the limited accuracy of the measured and/or predicted values for the three MRI parameters, and special effects like profile changes by enhanced diffusion and segregation as well as sputtering induced compound formation have not yet been implemented.

Recent advances include application of the MRI model to changing mixing length, information depth and backscattering factor in AES when sputtering through interfaces.

Acknowledgement

One of the authors (Siegfried Hofmann) has had the honor of being for three years the colleague of Dr. Kazuhiro Yoshihara at the National Research Institute for Metals (NRIM, now NIMS, National institute for Materials Science) in Tsukuba, Japan. Much of research work on the MRI model performed there could not have been carried out without the constant support and encouragement of Dr. Yoshihara, and beyond that, his cooperation and friendship are gratefully acknowledged.

References

- [1] K. Yoshihara, M. Yoshitake, *Surf. Interface Analysis* 18, 724(1992).
- [2] A. Benninghoven, *Z. Phys.* 230, 403 (1971).
- [3] S. Hofmann, *Appl. Phys.* 9, 59 (1976).
- [4] M.P. Seah, J.M. Sanz, S. Hofmann, *Thin Solid Films* 81, 239(1981).
- [5] S. Hofmann, *J. Vac. Sci. Technol.* A9, 1466 (1991).
- [6] S. Hofmann, in: S.G. Davison, ed., *Progress in Surface Science* Vol. 36, 35 (1991).
- [7] S. Hofmann, *J. Vac. Sci. Technol.* B10, 316 (1992).
- [8] S. Hofmann, *Surf. Interface Anal.* 21, 673 (1994).
- [9] ISO-14606.
- [10] S. Hofmann, *Rep. Prog. Phys.* 61, 827 (1998).
- [11] S. Hofmann, K. Yoshihara, *J. Surf. Anal.* 5, 40 (1999).
- [12] S. Hofmann, Jy Wang, *J. Surf. Anal.* 10, 52 (2003).
- [13] S. Hofmann, *Appl. Surf. Sci.* 241, 113 (2005).
- [14] P.C. Zalm, *Rep. Progr. Phys.*, 58 1321 (1995).
- [15] A. Rar, S. Hofmann, K. Yoshihara, K. Kajiwara, *Appl. Surf. Sci.* 144-145, 310 (1999).
- [16] A. Rar, I. Kojima, D. W. Moon, S. Hofmann, *Thin Solid Films* 355/356, 390 (1999).
- [17] S. Hofmann, *Surf. Interface Anal.* 27, 825 (1999).
- [18] S. Hofmann, *Thin Solid Films* 398-399, 336 (2001).

- [19] S. Hofmann, A. Rar, D. W. Moon, K. Yoshihara, *J. Vac. Sci. Technol. A* 19, 1111 (2001).
- [20] K. L. Yeo, A.T.S. Wee, R. Liu, C.M. Ng and A. See, *Surf. Interface Anal.* 33, 373 (2002).
- [21] K. L. Yeo, PhD Thesis, *National University of Singapore* 2004.
- [22] A. Takano, Y. Homma, Y. Higashi, H. Takenaka, S. Hayashi, K. Goto, M. Inoue, R. Shimizu, *Appl. Surf. Sci.* 203-204, 294 (2003).
- [23] K. Shimizu, R. Payling, H. Habazaki, P. Skeldon, G. E. Thompson, *J. Anal. At. Spectrom.* 19, 692 (2004).
- [24] S. Hofmann, *Surf. Interface Anal.* 30, 228 (2000).
- [25] T. Bungo, Y. Mizuhara, T. Nagatomi, Y. Takai, *Jpn. J. Appl. Phys.* 42, 7580 (2003).
- [26] S. Hofmann, Chap. 4 in *Practical Surface Analysis*, 2nd ed., D. Briggs and M.P. Seah, eds, Vol.1: AES and XPS, Wiley, Chichester 1990. p. 152.
- [27] S. Hofmann and J.Y. Wang, to be published in *Surf. Interface Anal.*
- [28] T. Wagner, J.Y. Wang and S. Hofmann, chap. 22 in: D. Briggs and J. T. Grant, eds., *Surface Analysis by Auger and X-ray Photoelectron Spectroscopy*, IM Publ., Chichester 2003, pp. 619-649.
- [29] P. Prieto, S. Hofmann, E. Elizalde, J.M. Sanz, *Surf. Interface Anal.* 36, 1392 (2004).
- [30] S. Hofmann, J. Y. Wang, *J. Surface Analysis* 9, 306 (2002).
- [31] S. Hofmann, A. Zalar, *Thin Solid Films* 60, 201 (1979).
- [32] A. Zalar, J. Kovač, B. Praček, S. Hofmann, P. Panjan, *Appl. Surf. Sci.* 252, 2056 (2005).
- [33] S. Hofmann, *Mikrochim. Acta Suppl.* 8, 71 (1979).